ACS Catalysis

Research Article

pubs.acs.org/acscatalysis

Mechanistic Insights into the Catalytic Oxidation of Carboxylic Acids on Au/TiO_2: Partial Oxidation of Propionic and Butyric Acid to Gold Ketenylidene through Unsaturated Acids

Monica McEntee,[†] Wenjie Tang,[‡] Matthew Neurock,[†,‡] and John T. Yates, Jr.*[,†,‡]

[†]Department of Chemistry, [‡]Department of Chemical Engineering, University of Virginia, Charlottesville, Virginia 22904, United States

Supporting Information

ABSTRACT: The partial oxidation of model C_2−C_4 (acetic, propionic, and butyric) carboxylic acids on Au/TiO_2 catalysts consisting of Au particles ∼3 nm in size was investigated using transmission infrared spectroscopy and density functional theory. All three acids readily undergo oxidative dehydrogenation on Au/TiO_2. Propionic and butyric acid dehydrogenate at the C2−C3 positions, whereas acetic acid dehydrogenates at the C1−C2 position. The resulting acrylate and crotonate intermediates are subsequently oxidized to form β-keto acids that decarboxylate. All three acids form a gold ketenylidene intermediate, $Au_2C{=}C{=}O$, along the way to their full oxidation to form CO_2. Infrared measurements of $Au_2C{=}C{=}O$ formation as a function of time provides a surface spectroscopic probe of the kinetics for the activation and oxidative dehydrogenation of the alkyl groups in the carboxylate intermediates that form. The reaction proceeds via the dissociative adsorption of the acid onto TiO_2, the adsorption and activation of O_2 at the dual perimeter sites on the Au particles (Au−O−O-Ti), and the subsequent activation of the C2−H and C3−H bonds of the bound propionate and butyrate intermediates by the weakly bound and basic oxygen species on Au to form acrylate and crotonate intermediates, respectively. The C=C bond of the unsaturated acrylate and crotonate intermediates is readily oxidized to form an acid at the beta (C3) position, which subsequently decarboxylates. This occurs with an overall activation energy of 1.5−1.7 ± 0.2 eV, ultimately producing the $Au_2C{=}C{=}O$ species for all three carboxylates. The results suggest that the decrease in the rate in moving from acetic to propionic to butyric acid is due to an increase in the free energy of activation for the formation of the $Au_2C{=}C{=}O$ species on Au/TiO_2 with an increasing size of the alkyl substituent. The formation of $Au_2C{=}C{=}O$ proceeds for carboxylic acids that are longer than C_2 without a deuterium kinetic isotope effect, demonstrating that C−H bond scission is not involved in the rate-determining step; the rate instead appears to be controlled by C−O bond scission. The adsorbed $Au_2C{=}C{=}O$ intermediate species can be hydrogenated to produce ketene, $H_2C{=}C{=}O(g)$, with an activation energy of 0.21 ± 0.05 eV. These studies show that selective oxidative dehydrogenation of the alkyl side chains of fatty acids can be catalyzed by nanoparticle Au/TiO_2 at temperatures near 400 K.

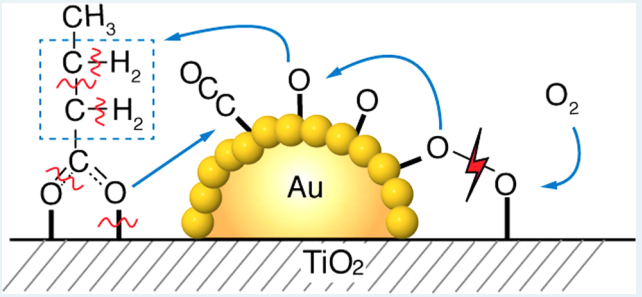

KEYWORDS: *Au/TiO_2, catalysis, oxidative-dehydrogenation, carboxylic acid oxidation, decarboxylation, ketenylidene*

1. INTRODUCTION

Biomass, in the form of carbohydrates, oils, and fatty acids, can be converted into key chemical intermediates to replace nonrenewable fossil fuel resources used in the synthesis of different chemicals and fuels.[1] Recent studies on the decarbonylation and decarboxylation of model carboxylic acids over transition metal catalysts have generated significant interest because of their potential application in the conversion of fatty acids to olefins at low temperatures.[2−6] Experimental studies[4−7] and theoretical studies on model linear carboxylic acids[8,9] suggest that the decarboxylation proceeds via an initial activation and dehydrogenation of C_2−H and C_3−H bonds before undergoing C−O or C−C bond scission over Pd catalysts; however, only a few studies are found for carboxylic acid oxidation on Au-based catalysts.[10−12]

Au nanoparticles supported on metal oxides have been shown to enhance catalytic activity for many oxidation reactions,[13−19] including CO oxidation[20−27] and olefin oxidation,[28] in which the active sites for catalysis are found to reside at the Au/TiO_2 interface. Green et al.[10,11] studied the oxidation of ethylene and acetic acid on a Au/TiO_2 catalyst and found that both molecules result in the formation of the partially oxidized gold ketenylidene species, $Au_2C{=}C{=}O$, via a sequence of kinetic steps involving the deprotonation of the acid at the Ti sites to form the acetate intermediate, the activation of two of the C−H bonds of the terminal CH_3 group

Received: September 18, 2014
Revised: December 10, 2014
Published: December 12, 2014

DOI: 10.1021/cs5014255
ACS Catal. 2015, 5, 744−753

by bound O* or OH* intermediates and the subsequent scission of the C−O bond at the bifunctional Ti−Au site to form the $Au_2C{=}C{=}O$ intermediate.

Exploratory studies on the oxidation of larger carboxylic acids such as propionic and butyric acid on a Au/TiO_2 catalyst were recently reported.[12] Here, we present detailed in situ FTIR observations of C−C bond cleavage at the second (C2) and third (C3) carbons, which reside at the α and β positions from the −COO group of both the propionate and butyrate species, followed by C−O bond cleavage in −COO to produce $Au_2C{=}C{=}O$ species at the Au/TiO_2 perimeter sites. Density functional theory (DFT) calculations show that dehydrogenation at the C_α-C_β bond occurs before the C−C bond scission in a manner similar to the decarboxylation of propionic acid over the Pd(111) surface.[8,9] Detailed in situ FTIR isotopic kinetic experiments combined with DFT calculations help to elucidate the reaction mechanism for the production of the $Au_2C{=}C{=}O$ species from both C_3- and C_4-carboxylate species. The present study on the kinetics for the oxidative dehydrogenation and decarboxylation of propionic and butyric acid to produce ketenylidene on a Au/TiO_2 catalyst extends a very brief earlier report on the initial dehydrogenation of these acids.[12]

2. PROCEDURAL METHODS

2.1. Experimental Section. A high vacuum transmission IR cell with a base pressure of $\sim 1 \times 10^{-8}$ Torr was employed, and a detailed description is provided elsewhere.[19,20,29] The Au/TiO_2 catalyst was synthesized using a deposition−precipitation procedure provided by Zanella et al.,[30] yielding Au particles with an average diameter of ~3 nm[20] and a weight percentage of Au of 8%. Acetic acid (≥99.7%, ACS reagent), propionic acid (≥99.5%, ACS reagent), propionic-3,3,3-d_3 acid (99 atom % D), propionic-2,2-d_2 acid (98 atom % D), butyric acid (≥99.5%, analytical standard), and butyric-d_7 acid (98 atom % D) were acquired from Sigma-Aldrich and purified using the freeze−pump−thaw method. Gas and liquid purity analysis were performed using a quadrupole mass analyzer attached to the IR cell. The isotopically labeled propionic acid samples were also characterized using ^{1}H NMR analysis and an external GC/MS spectrometer (Thermo Finnigan Voyager MS with Trace 2000 GC) verifying their stated isotopic purity.

The catalyst was pretreated with ~18 Torr of O_2(g) at 473 K for ~3.5 h before each experiment to remove any hydrocarbon impurities. After evacuation of the O_2 gas, ~2 Torr of H_2(g) was introduced into the cell for 10 min, followed by evacuation. H_2(g) removes O adatoms that originated from O_2 pretreatment on Au and TiO_2 sites to form H_2O, which then desorbs from the surface at 473 K. The catalyst was then cooled to the desired temperature. Approximately 0.4 Torr of carboxylic acid vapor was introduced into the cell and then evacuated for 30 min. One Torr of O_2(g) was then introduced into the cell, and a FTIR spectrum was taken every minute for 2.5 h. Each FTIR spectrum took 52s and contained 128 scans at 2 cm^{-1} resolution. The $Au_2C{=}C{=}O$ absorbance increase was used to evaluate the kinetics of the oxidation process.

For the hydrogenation experiments, after the carboxylate species were oxidized, forming $Au_2C{=}C{=}O$, and the cell was evacuated, the catalyst was cooled to 292 K and exposed to 1 Torr of H_2(g) for 10 min at various temperatures. Hydrogenation of the unsaturated products on the surface was followed by FTIR.

2.2. Theoretical. First principle periodic plane wave DFT calculations implemented in the Vienna Ab Initio Simulation Program[31] were carried out to determine the activation energies and reaction energies associated with the reaction pathways. The results were used to examine proposed mechanisms for the oxidation of propionic acid over a model Au/TiO_2 interface.

A (2 × 3) unit cell with four O−Ti−O trilayers was used to model the rutile TiO_2(110) surface. The experimental 3 nm Au particles on TiO_2 were simulated by using a close-packed Au nanorod anchored to a model TiO_2(110) surface. This model provides various interfacial Au and Ti sites and has proven to be reliable in mimicking important properties of supported Au in different previous studies.[11,17,20,27] The top two trilayers of the TiO_2 surface were allowed to fully relax while the atoms in the bottom two trilayers of the TiO_2 slab were fixed to their lattice positions to mimic the bulk. All of the Au atoms in the nanorod were allowed to relax in the z direction to maintain good lattice matching with the oxide surface. All of the calculations reported herein were carried out using the PW91 exchange correlation functional.[32] The projector augmented-wave (PAW) method was used to simulate the core electrons.[33,34] The valence electrons were described with Kohn−Sham single-electron wave functions and expanded in plane-wave basis with energy cutoff of 400 eV. The DFT+U method was employed to correct the on-site Coulomb interactions with U = 4.0 eV to generate experimentally observed electronic structures.[35,36] More details of the model structure and calculation can be found in the Supporting Information (SI).

3. RESULTS AND DISCUSSION

3.1. IR Frequencies of Carboxylic Acid Conversion to Acetate, Propionate, and Butyrate Along with Ketenylidene Formation at 400 K on the Au/TiO_2 Catalyst. The results for the oxidation of the three carboxylic acids (acetic acid, propionic acid, and butyric acid) carried out at 400 K on Au/TiO_2 are shown in Figure 1. For each experiment, 0.4 Torr of acid vapor was introduced into the cell for adsorption to saturation coverage, and the cell was then evacuated for 30 min. The black curves reported in Figure 1 correspond to the

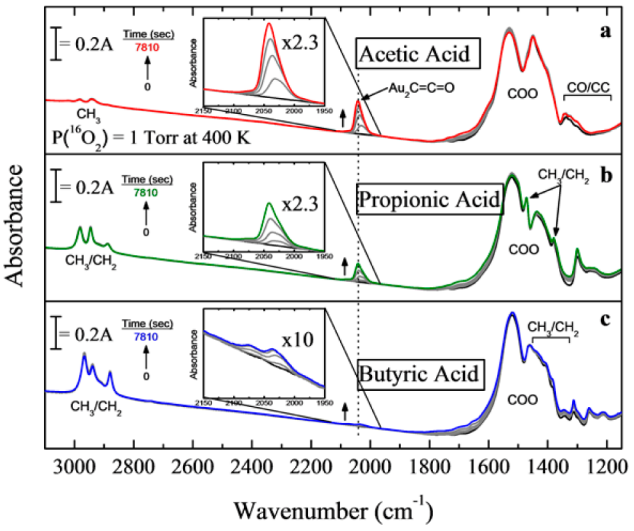

Figure 1. IR spectra comparison of (a) acetic acid, (b) propionic acid, and (c) butyric acid oxidation on Au/TiO_2 at 400 K for 7810 s. The black spectra were taken before adding O_2 to the IR cell, and the red (a), green (b), and blue (c) curves were taken after 7810 s in O_2.

DOI: 10.1021/cs5014255
ACS Catal. 2015, 5, 744−753

spectrum before oxidation, with the acid already present on the surface. Figure 1a (black curve) shows acetic acid (CH_3COOH) on Au/TiO_2 at 400 K. In agreement with previously reported assignments by Green et al.[10,11] and others,[37−39] acetic acid dissociates to form acetate (CH_3COO) species on TiO_2 with IR bands at 2936 ($\nu_s(CH_3)$), 1532 ($\nu_{as}(CO_2)$), 1454 ($\nu_s(CO_2)$), and 1338 ($\delta(CH_3)$) cm^{-1}. Similarly, propionic acid (CH_3CH_2COOH) dissociates to produce propionate (CH_3CH_2COO) species on TiO_2, as shown in Figure 1b (black curve) with major bands at 2981 ($\nu_{as}(CH_3)$), 2946 ($\nu_{as}(CH_3)$ in Fermi resonance/$\nu_{as}(CH_2)$), 2888 ($\nu_s(CH_3)/\nu_s(CH_2)$), 1523 ($\nu_{as}(CO_2)$), 1473 ($\delta_{as}(CH_3)$), 1430 ($\nu_s(CO_2)$), 1380 ($\delta_s(CH_3)$), and 1300 ($\delta(CH_2)$) cm^{-1}, which are in agreement with literature frequencies.[40]

Following the same trend, as shown in Figure 1c (black curve), the butyric acid ($CH_3CH_2CH_2COOH$) IR spectrum displays bands at 2967 ($\nu_{as}(CH_3)$), 2939 ($\nu_{as}(CH_3)$ in Fermi resonance/$\nu_{as}(CH_2)$), 2880 ($\nu_s(CH_3)/\nu_s(CH_2)$), 1522 ($\nu_{as}(CO_2)$), 1461 ($\delta_{as}(CH_3)$), 1408 ($\nu_s(CO_2)$), and 1382 ($\delta_s(CH_3)$) cm^{-1}, which are assigned to butyrate ($CH_3CH_2CH_2COO$) species on TiO_2.[41−43] The same bands mentioned above for all three acids were seen on the blank TiO_2 catalyst (see SI Figure S1), confirming that the carboxylate species adsorb on the TiO_2 sites alone. All three of these carboxylic acids show a similar well-known trend, with the initial step in adsorption involving the deprotonation of the −COOH group[44,45] on TiO_2 sites, followed by adsorption of the carboxylate species, which provides a common starting point for the oxidation of these carboxylate species.

The next steps in the oxidation mechanism involve O_2 dissociation at the Au/TiO_2 interface to result in the formation of weakly bound O adatoms on Au that are negatively charged and act as a Lewis base in catalyzing the activation of weakly acidic C−H bonds, as described in our previous work.[12] The propionate (CH_3CH_2COO) and butyrate ($CH_3CH_2CH_2COO$) intermediates can react via an oxidative dehydrogenation of the $C_\alpha-C_\beta$ bonds to form surface acrylate ($CH_2{=}CHCOO$) and crotonate ($CH_3CH{=}CHCOO$) intermediates. These results are consistent with previous work by Green et al.[11] in which two H atoms were proposed to be sequentially removed from the methyl group of acetic acid by O adatoms during the first acetic acid oxidation steps on Au/TiO_2 to form the ketenyl CHCOO intermediate on Au.

Another IR band around 2040 cm^{-1} is observed to develop during the oxidation of acetate, propionate, and butyrate separately on Au/TiO_2 at 400 K, as shown in Figure 1 in the magnified inserts. This absorbance band was previously assigned to a gold ketenylidene species, $Au_2C{=}C{=}O$, by Green et al.[10,11] for acetic acid oxidation on Au/TiO_2. To produce this 2-carbon ketenylidene species from both propionate and butyrate, C−C bond breaking at the C2−C3 position must occur at a later stage in the oxidation process. All the experiments were repeated on the blank TiO_2 catalyst, and no ketenylidene species were formed, as shown in SI Figure S2. Because all three acids adsorb as carboxylate species on the TiO_2 support, the reaction likely takes place at the Au/TiO_2 perimeter to form C=C=O ketenylidene species, which are then adsorbed on Au sites.

Oxidation experiments were also performed using $^{18}O_2$ gas to verify the origin of the O atom in the final ketenylidene product. For both propionic and butyric acid, the main ketenylidene product was $Au_2C{=}C{=}{}^{16}O$, which is consistent with the C−C bond scission at the second and third carbons for both acids and the scission of one of the C−O bonds in the carboxylate on the TiO_2 support. The spectra are shown in the SI in Figure S3. The use of $^{18}O_2$ (g) led to very little or no formation of $Au_2C{=}C{=}{}^{18}O$. The possibility that the O atom comes from the TiO_2 lattice under vacuum conditions on Au/TiO_2 is also ruled out because before adding O_2 in each experiment, an IR spectrum was taken every minute for 30 min to monitor the changes on the surface. No ketenylidene was formed on the surface without O_2 gas being present in the cell, as shown in the SI in Figure S4. This observation is consistent with oxygen-induced activation of the C−H bonds, followed by C−O activation, leading to $Au_2C{=}C{=}O$.

3.2. Kinetic Studies of Ketenylidene Formation from Acetate, Propionate, and Butyrate under Oxidizing Conditions. Figure 2 displays the integrated absorbance at

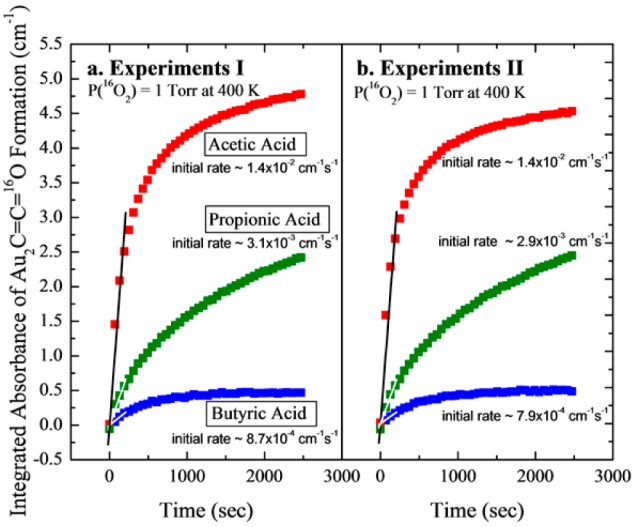

Figure 2. Two sets of kinetic studies of the $Au_2C{=}C{=}{}^{16}O$ formation from acetic acid (red curves), propionic acid (green curves), and butyric acid (blue curves) oxidation on Au/TiO_2 at 400 K. The black and white solid lines represent the initial rate fits for the experimental data.

2040 cm^{-1} of $Au_2C{=}C{=}{}^{16}O$ formation during oxidation over a period of 2500 s for all three acids at 400 K. Each set of experiments (I and II, performed to confirm reproducibility) in Figure 2a,b was carried out in a random order to ensure the integrity of the measurements. The second set of experiments in Figure 2b was also carried out to show the reproducible behavior of the catalyst after several cycles. The initial rates (black and white lines) of $Au_2C{=}C{=}{}^{16}O$ formation show a ~15-fold increase at 400 K for acetic acid compared with butyric acid for both sets of experiments. Propionic acid oxidation shows an intermediate behavior. This rate change in $Au_2C{=}C{=}{}^{16}O$ formation is likely due to changes in the activation enthalpy or the activation free energy to form the $Au_2C{=}C{=}O$ intermediate.

To determine the reason for this trend, we carried out propionate oxidation experiments at various temperatures between 400 and 440 K and butyrate oxidation experiments at temperatures between 400 and 420 K, as shown in Figure 3a,b. This temperature range was chosen to avoid slow kinetics at 370 K (lowest tested temperature that shows $Au_2C{=}C{=}{}^{16}O$ formation) and to avoid desorption or decomposition of the ketenylidene species at temperatures above 440 K. The initial rate of each reaction was fit to a first-order kinetic model

DOI: 10.1021/cs5014255
ACS Catal. 2015, 5, 744−753

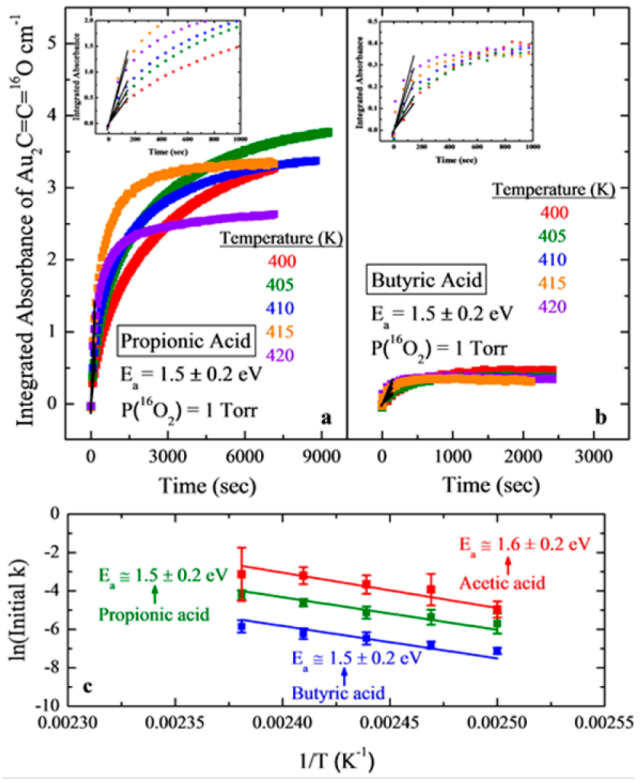

Figure 3. Integrated absorbance plots of $Au_2C{=}C{=}{}^{16}O$ formation during oxidation at different temperatures are fitted to initial rate kinetics for (a) propionic acid and (b) butyric acid. (c) The activation energies of formation from acetic acid (red), propionic acid (green), and butyric acid (blue) are compared in the Arrhenius plot. Data for acetic acid were taken from ref 11.

to obtain a rate constant, k. Figure 3c shows the Arrhenius plots used to calculate the activation energies, E_a, for each acid. The acetic acid data were obtained from previous experiments performed by Green et al.[11] The slopes of the lines for ln(initial rate) vs $1/T$ (K^{-1}) for $Au_2C{=}C{=}{}^{16}O$ formation from propionate and butyrate reported in Figure 3c were used to calculate activation barriers of 1.5 ± 0.2 eV for both 3- and 4-carbon carboxylate species, which are similar to the observed E_a of 1.6 ± 0.2 eV for $Au_2C{=}C{=}{}^{16}O$ formation from acetic acid. The similarity in E_a values implies the change in rates in Figure 2 for the three carboxylates is not the result of simple differences in the apparent activation energy (E_a) in the $Au_2C{=}C{=}{}^{16}O$ formation process, where barrier differences are proposed to govern the rates of the oxidation of the three carboxylate species.

The measured rate constants, shown in Figure 3, decrease in magnitude as one proceeds from acetate to propionate to butyrate while exhibiting similar activation energies. The reaction proceeds forward at slower rates as the alkyl group becomes more bulky. This observation indicates that the changes in rate are not due to changes in the enthalpies of activation but may be the result of entropic changes. We examine the changes in entropy and free energy in more detail in section 3.5.

3.3. Deuterium Kinetic Isotope Effect (DKIE) Study of Propionate and Butyrate During Oxidation on the Au/TiO_2 Catalyst. To determine if C−H bonds are involved in the rate-determining step of the oxidative dehydrogenation reaction, we performed the same oxidation experiments at 400 K using deuterated propionic acid. Figure 4a shows the integrated absorbance of the $Au_2C{=}C{=}{}^{16}O$ formation as a

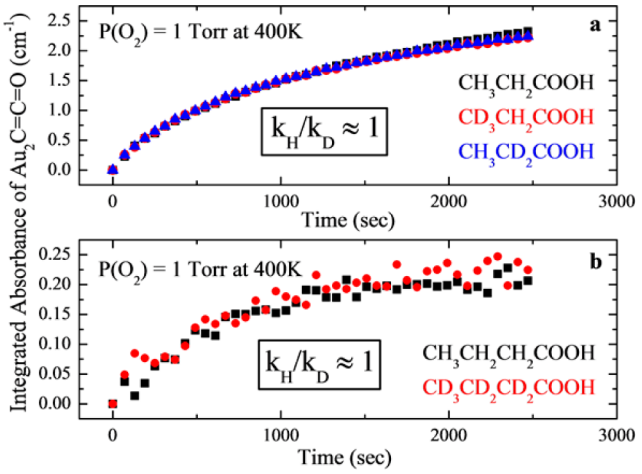

Figure 4. Kinetic plots of the integrated absorbance of $Au_2C{=}C{=}O$ formation from (a) CH_3CH_2COOH (black), CD_3CH_2COOH (red), and CH_2CD_2COOH (blue) oxidation on Au/TiO_2 at 400 K; (b) $CH_3CH_2CH_2COOH$ (black) and $CD_3CD_2CD_2COOH$ (red) oxidation on Au/TiO_2 at 400 K.

function of time for both deuterated propionic acids (CD_3CH_2COOH (red curve) and CH_3CD_2COOH (blue curve)) and propionic acid (CH_3CH_2COOH (black curve)). The deuterated acid oxidation experiments were performed in exactly the same way as previously employed, with the CH_3CH_2COOH data taken from Figure 2 and redisplayed here. To accurately determine the k_H/k_D ratio, a 3-point slope at every data point was obtained for all acids, and the k_H/k_D ratio was evaluated at each point. The average k_H/k_D ratio is unity to within ±10% for both deuterated acids at all levels of completion of the reaction. For CD_3CH_2COOH and CH_3CD_2COOH, the kinetic involvement of D also does not change the rates, meaning that the activation step for conversion to $Au_2C{=}C{=}{}^{16}O$ does not involve C−H bond scission at either the second or third carbon atoms.

Similarly, Figure 4b displays the rates of $Au_2C{=}C{=}{}^{16}O$ formation for both fully deuterated butyric acid ($CD_3CD_2CD_2COOH$ (red curve)) and butyric acid ($CH_3CH_2CH_2COOH$ (black curve)). The average k_H/k_D ratio is unity for the deuterated butyric acid, as well. According to all of the plots, no DKIE exists for propionic acid with D labeling on either carbon atom or for fully deuterated butyric acid. This means that C−H bond scission is not involved in the rate-determining step in the catalytic oxidation of the larger acids to produce $Au_2C{=}C{=}O$. In contrast, for CH_3COOH to form $Au_2C{=}C{=}{}^{16}O$, a DKIE of ∼4 was found.[11] Detailed theoretical and kinetic analyses showed that although C−O activation was the rate-controlling step for the selective oxidation of acetic acid, the C−H activation steps preceding the C−O scission were not quasi-equilibrated, thus resulting in kinetic differences between the rates of oxidation of deuterated and nondeuterated acetic acid to form $Au_2C{=}C{=}{}^{16}O$ and a DKIE value of ∼4.[11]

3.4. Kinetic Studies of Ketenylidene Hydrogenation. To understand the later intermediate steps in the oxidation mechanism leading to $Au_2C{=}C{=}O$ formation, we approached the problem by starting with the final stable, observable surface-

DOI: 10.1021/cs5014255
ACS Catal. 2015, 5, 744−753

bound product, ketenylidene. Once the ketenylidene was formed from the oxidation of propionate and the O_2 was evacuated from the cell, the catalyst was cooled to 292 K and exposed to 1.0 Torr of H_2 for 10 min at various temperatures. The FTIR spectra are shown in Figure 5a of the $Au_2C{=}C{=}O$ species after 10 min in the temperature range of 292−350 K. The decreasing peak absorbance at 2040 cm^{-1} is attributed to the hydrogenation of ketenylidene to produce ketene ($H_2C{=}C{=}O$) in the gas phase. A temperature-programmed desorption experiment confirms the production of ketene in the gas phase (see SI Figure S5). Figure 5b shows the normalized integrated absorbance plots of ketenylidene hydrogenation at various temperatures fitted to first-order kinetics to determine the E_a for hydrogenation. The Arrhenius plot in Figure 5 insert c yields E_a = 0.21 ± 0.05 eV.

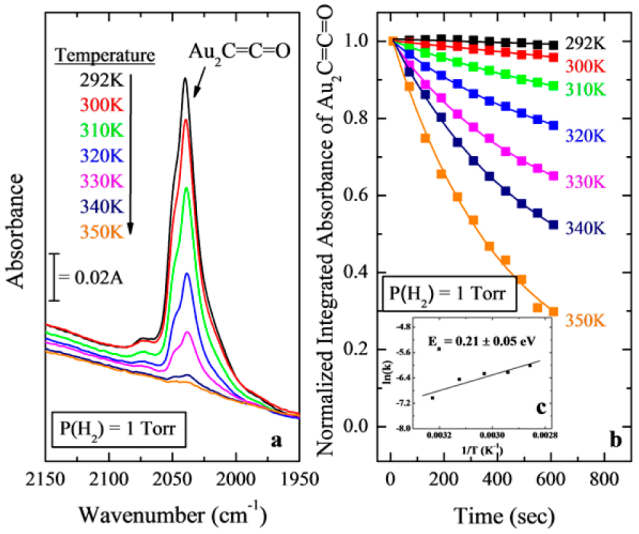

Figure 5. (a) IR spectra of $Au_2C{=}C{=}O$ after 10 min in 1 Torr of H_2 at various temperatures on Au/TiO_2. (b) Normalized integrated absorbance plots of $Au_2C{=}C{=}O$ hydrogenation at various temperatures. The solid lines represent the first-order kinetic fits for the experimental data. Insert (c) shows the Arrhenius plot and activation energy of ketenylidene hydrogenation.

This low activation barrier is consistent with a weak interaction between the ketene species and the Au surface. At the temperatures used in the oxidation experiments (400−440 K), this low activation barrier would allow for the $H_2C{=}C{=}O$ species to desorb from the surface before the final $C{=}C{=}O$ species could form on the Au. Therefore, we conclude that after C−C bond scission, the last steps in the oxidation mechanism are the formation of either the $C{=}C{=}O$ species or an intermediate $HC{=}C{=}O$ species on Au which then dehydrogenates to form the $C{=}C{=}O$ product chemisorbed on Au. The adsorbed ketene is not a precursor to $Au_2C{=}C{=}O$. These steps indicate that the C_α−H bonds must be activated before C−C and C−O bond scission, which is consistent with the early dehydrogenation steps to form C=C moieties at the second and third carbon atoms.[12]

3.5. Density Functional Theory Simulations of Propionate C−C Bond Scission to Form Ketenylidene.

DFT calculations were carried out to examine plausible reaction pathways and the possible mechanism for the formation of ketenylidene from the propionate as well as the butyrate intermediates. The calculated energy diagram for ketenylidene formation from the adsorbed propionate is shown in Figure 6. The detailed atomic structures for all of the species involved in the network are depicted in Figure S6 in the SI. As reported previously,[20] O_2 activation is thought to occur on dual $Au{-}Ti^{4+}$ sites at the Au/TiO_2 interface. The activation energy for O−O bond breaking in the absence of CO at the $Au{-}Ti^{4+}$ site was calculated to be 0.5 eV. The O adatoms that result can diffuse to other sites on the Au surface with diffusion barriers ranging

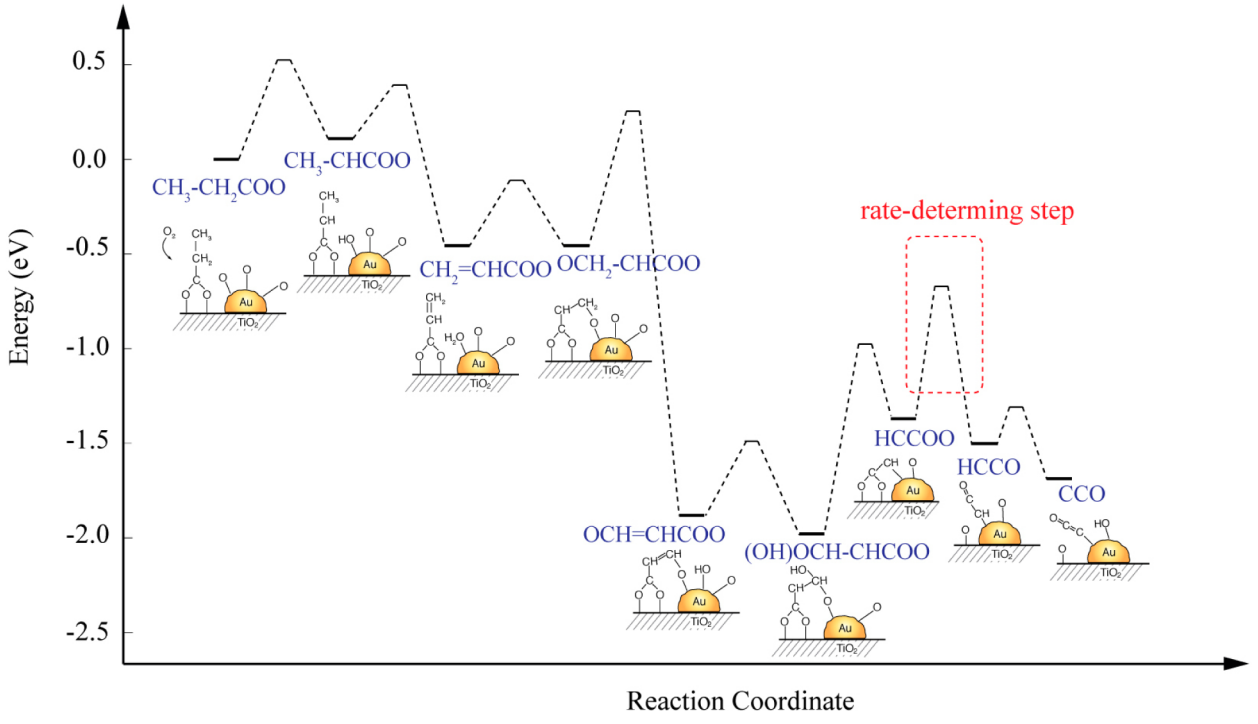

Figure 6. DFT-calculated reaction energy diagram for the oxidation of propionate to ketenylidene.

DOI: 10.1021/cs5014255
ACS Catal. 2015, 5, 744−753

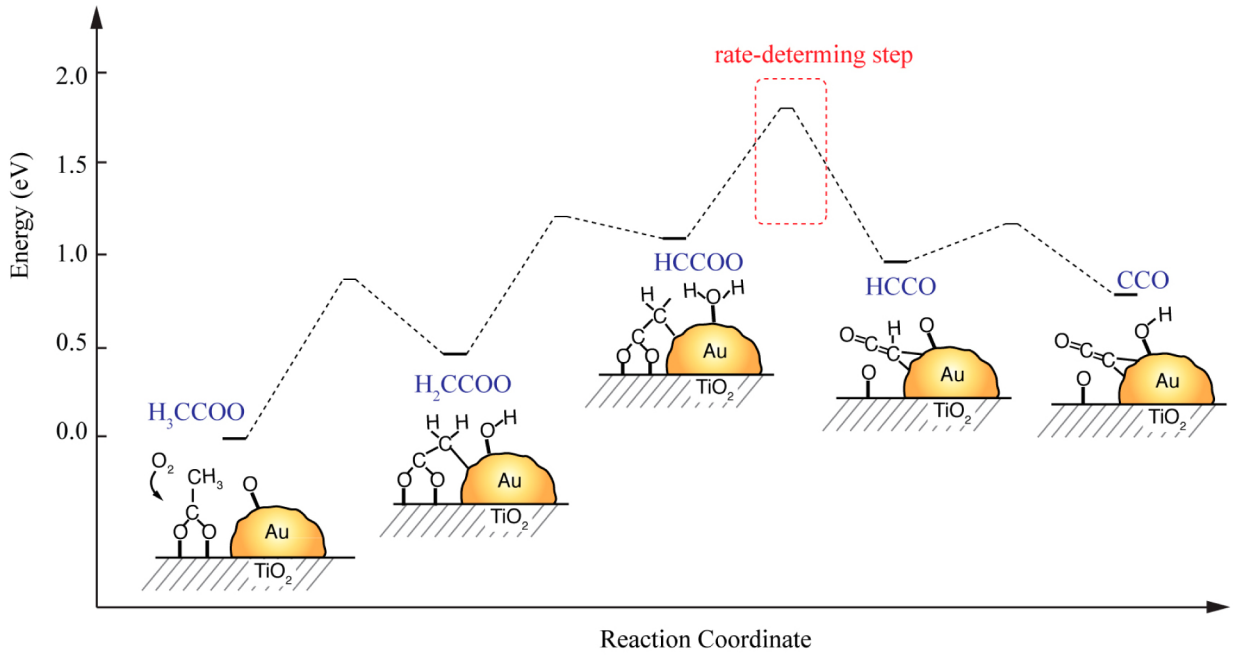

Figure 7. DFT-calculated reaction energy diagram for the oxidation of acetate to ketenylidene.

from 0.2 to 0.7 eV.[21] O_2 can also be activated at defect sites such as a Ti interstitial,[46,47] which has an activation barrier similar to that at the Au−Ti^{4+} site. The atomic O that results on Au is weakly held and behaves as a base where it can carry out nucleophilic attack on the unsaturated C═C bonds and, in addition, activates weakly acidic C−H bonds.[48−53] These basic O species on Au were shown previously to play an important role in the oxidation of both ethylene and acetate on Au/TiO_2.[11,28]

A range of different elementary reaction steps and possible mechanisms for producing ketenylidene from propionate were examined. Herein, we discuss only the lowest energy and most favorable path. The lowest energy route proceeds with the activation of the α-C−H bonds of $CH_3CH_2COO^{*Ti}$ by O (eq 1) or OH (eq 2) on Au with activation barriers of 0.53 and 0.28 eV, respectively, and reaction energies of 0.12 and −0.57 eV, respectively, resulting in acrylate (CH_2═CH−COO^{*Ti}) and H_2O. H_2O, which is weakly bound to Au with an adsorption energy of −0.08 eV, readily desorbs at 400 K.

$$CH_3CH_2COO^{*Ti} + O^{*Au} \rightarrow CH_3CHCOO^{*Ti} + OH^{*Au} \quad (1)$$

$$CH_3CHCOO^{*Ti} + OH^{*Au} \rightarrow CH_2{=}CHCOO^{*Ti} + H_2O^{*Au} \quad (2)$$

The ^{*Ti}, ^{*Au}, and ^{*TiAu} symbols used herein refer to the specific adsorption sites (Ti, Au, and bifunctional Ti−Au) at the Au/TiO_2 interface.

The initial C−H activation of propionate (0.46 eV) at the α-C−H bond to form CH_3CHCOO^{*Ti} was found to be 0.4 eV more favorable than the activation of the same α-C−H bond of acetate (0.86 eV, Figure 7).[11] The reaction energies for both reactions are endothermic and follow the same trend. The lower barrier and more favorable reaction energies for propionate are due to the stabilization that results upon activating a secondary C−H bond, as opposed to a terminal C−H bond. Although the subsquent activation of the β-C−H bond of CH_3CHCOO^{*Ti} to form CH_2═$CHCOO^{*Ti}$ is also favored over the α-C−H bond of the CH_2COO^{*TiAu} intermediate to form $CHCOO^{*TiAu}$, the reaction energies for these steps are characteristically different in that the reaction to form the stable CH_2═$CHCOO^{*Ti}$ acrylate intermediate is exothermic by −0.57 eV, whereas the reaction energy to form the CH═COO^{*Ti} product is actually endothermic. The lower barriers and the shift to exothermic reaction energies for C_3 over the C_2 intermediates are due to the stabilization that results in forming a terminal olefin in the acrylate product for C_3, C_4, and longer acids.

The reactivity of the acrylate (CH_2═$CHCO_2{}^{*Ti}$) product from propionate is quite different from that of the $CHCOO^{*TiAu}$ species from acetate. The later proceeds by the direct activation of the CO bond to form HC═C═O^{*Au}, which goes on to form the ketenylidene intermediate directly (Figure 7). The unsaturated C═C bond in acrylate, on the other hand, readily undergoes nucleophilic attack by the weakly held and basic O on Au to form OCH_2−CH−COO^{*TiAu} (eq 3) with an activation barrier of 0.35 eV (Figure 6). A second O on Au can subsequently activate the C−H bond of the terminal OCH_2− group to form OCH═$CHCOO^{*TiAu}$ and OH^{*Au} (eq 4) with a barrier of 0.75 eV. The resulting OH^{*Au} can then attack the terminal O═CH− group to form the (OH)OCH−$CHCOO^{*TiAu}$ (eq 5) intermediate with a barrier of 0.39 eV.

$$CH_2{=}CHCOO^{*Ti} + O^{*Au} \rightarrow OCH_2 - CHCOO^{*TiAu} \quad (3)$$

$$OCH_2 - CHCOO^{*TiAu} + O^{*Au} \rightarrow OCH{=}CHCOO^{*TiAu} + OH^{*Au} \quad (4)$$

$$OCH{=}CHCOO^{*TiAu} + OH^{*Au} \rightarrow (OH)OCH - CHCOO^{*TiAu} \quad (5)$$

C−C bond activation takes place after the formation of (OH)OCH−$CHCOO^{*TiAu}$ (eq 6) and proceeds with a barrier of 1.00 eV and generates formic acid, $HCOOH^{*Au}$, as well as

DOI: 10.1021/cs5014255
ACS Catal. 2015, 5, 744−753

the HCCOO*^{TiAu} products that form at the sites along the perimeter of Au/TiO_2. The C−C bond-breaking mechanism found herein is consistent with previous reports.[54,55] The carboxylate group (−COO*^{TiAu}) that anchors the (OH)OCH−$C^{(\alpha)}HC^{(\beta)}OO$*^{TiAu} intermediate to the TiO_2 support sits β to the terminal acid ((OH)OC−) and facilitates the direct C−C bond scission and decarboxylation of the β-keto acid ((OH)-OC−). The HCOOH*^{Au} that forms binds weakly to a Au edge site and can readily desorb with an energy of 0.25 eV. The HCCOO*^{TiAu} fragment that results can subsequently undergo C−O bond scission (eq 7) with a barrier of 0.71 eV to form the HC═C═O*^{Au} intermediate. This changes the binding mode for the HCCOO*^{TiAu} reactant from a bidentate interaction involving terminal O−Ti and HC−Au interactions to a monodentate HC−Au interaction for the HC═C═O*^{Au} product. The HC═C═O*^{Au} can then react with O on Au to form the final Au_2C═C═O product (eq 8) with a barrier of 0.21 eV.

$$(OH)OCH - CHCOO^{*TiAu} \rightarrow HCOOH^{*Au} + HCCOO^{*TiAu} \quad (6)$$

$$HCCOO^{*TiAu} \rightarrow HC{=}C{=}O^{*Au} + O^{*Ti} \quad (7)$$

$$HC{=}C{=}O^{*Au} + O^{*Au} \rightarrow C{=}C{=}O^{*Au} + OH^{*Au} \quad (8)$$

The intrinsic activation barriers for all steps described above range from 0.21 to 1.00 eV, consistent with the fact that the carboxylic acid oxidation reaction readily occurs at a temperature of 400 K. To summarize, the reaction path reported here involves the activation of O_2 at the bifunctional Au−Ti^{4+} sites to generate weakly held O atoms on Au. These species are basic in character and, as such, aid in the activation of weakly acidic C−H bonds and readily undergo nucleophilic addition of oxygen to the unsaturated C═C bonds of acrylate and crotonate to form β-carboxylate acids, which promote the direct decarboxylation and C−O bond activation steps that occur at the interfacial sites for Au/TiO_2. The steps reported here were calculated to be the lowest energy path to form the ketenylidene.

A similar mechanism and set of paths were examined for the selective oxidation and decarboxylation of the adsorbed butyrate intermediate, which are shown in detail in Figures S8−S9 in the Supporting Information. The results show energetics very similar to those found for the adsorbed propionate. Although the overall paths presented herein are consistent with experimental results, the relative ordering of the individual elementary steps and the exact nature of each step could be different. This should not, however, affect the overall conclusions.

The reaction energy diagram depicted in Figure 6 shows that the activation of propionate in general proceeds downhill via a sequence of intrinsic C−H activation and O and OH addition steps with relatively low intrinsic activation barriers between 0.5 and 0.75 eV to form the (OH)OCH−CHCOO*^{TiAu} species. The (OH)OCH−CHCOO*^{TiAu} intermediate resides in a deep energy well due to the high exothermicity of the preceding C−H activation steps involving the oxidative dehydrogenation of CH_3−CH−COO*^{Au} to CH_2═CH−COO*^{Au} and OCH_2−CHCOO*^{TiAu} to O═CH−CHCOO*^{TiAu}, leading to the formation of very stable unsaturated olefinic or carbonyl groups. The resulting energies reported in Figure 6 suggest that the formation of (OH)OCH−CHCOO*^{TiAu} is quasi-equilibrated. The barrier to hydrogenate OCH═CHCOO*^{TiAu} back to form OCH_2−CHCOO*^{TiAu} is 2.19 eV, which is over 1 eV higher than the forward apparent activation barriers needed to activate the C−C bond of (OH)OCH−CHCOO*^{TiAu} (0.90 eV) or the C−O bond of HCCOO*^{Ti} (1.21 eV) in the kinetically relevant step. Although the results here are similar to those for the partial oxidation of acetate (Figure 7) in that the kinetically relevant step involves the activation of the C−O bond, they are characteristically different in that they involve the formation of a stable quasi-equilibrated surface intermediate prior to C−O activation to form the ketenylidene, as opposed to the reactions of acetate that proceed through the formation of the much less stable HCCOO*^{TiAu} intermediate.

A microkinetic model was constructed using the DFT-calculated adsorption and desorption energies, reaction energies, and activation barriers for the selective oxidation of propionic acid reported in eqs 1−8, along with preexponential values estimated from statistical mechanics and transition state theory. The resulting differential equations were solved to provide a more rigorous analysis of the resulting kinetics for the oxidation of propionic acid to form the ketenylidene. The simulations were carried out over a range of temperatures to calculate the apparent activation energy for ketenylidene formation to compare with the experiments. The results indicate that C−O activation and the availability of empty active sites control the rate of the reaction. An apparent activation energy of 1.58 eV was calculated from the microkinetic simulations, which is consistent with the value of 1.5 eV found experimentally.

As reported earlier, the large 15-fold increase in the experimental Au_2C═C═O formation rates reported in Figure 2 in moving from the smaller acetic acid to the larger butyric acid is not the result of differences in the activation enthalpies because the apparent activation barriers are all within <0.1 eV for reactions involving the same rate-determining C−O activation for all three acids, as was shown experimentally and theoretically. The calculated barriers reported in Figure 6, however, refer only to changes in the electronic energies and do not include changes that result from changes in internal molecular motions in the adsorbed species or entropic changes.

To provide a more rigorous analysis and comparison of the three different acids, we instead examine the changes in Gibbs free energy barriers at 400 K for the formation of Au_2C═C═O. This involved calculating the translational, rotational, and vibrational partition functions for the reactants and products for the three acids. In our system, the translational and rotational parts have essentially no contributions, because the species involved are strongly adsorbed on the catalyst surface.[17] Therefore, the free energy barrier can be calculated from the contributions of the electronic and vibrational partition function. The relation between the reaction rate k and the free energy barrier ΔG can be written as

$$k \sim \frac{k_B T}{h} \exp\left(-\frac{\Delta G}{k_B T}\right) \quad (9)$$

where T is the temperature, k_B is the Boltzmann constant, and h is the Planck constant. The Au_2C═C═O formation rate ratio for acetic acid (k_1) and propionic acid (k_2) can be expressed by

$$\frac{k_1}{k_2} = \exp\left(-\frac{\Delta G_1 - \Delta G_2}{k_B T}\right) \quad (10)$$

DOI: 10.1021/cs5014255
ACS Catal. 2015, 5, 744−753

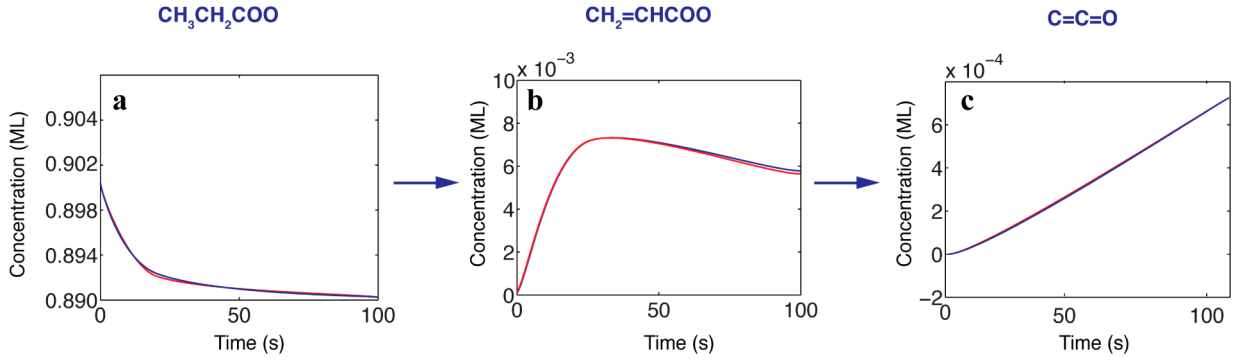

Figure 8. A comparison of surface concentrations of (a) CH_3CH_2COO (or CD_3CD_2COO), (b) $CH_2{=}CHCOO$ (or $CD_2{=}CDCOO$), and (c) C=C=O intermediates at the Au−Ti^{4+} interface as a function of time derived from microkinetic simulations carried out for the partial oxidation of deuterium labeled and unlabeled adsorbed propionate.

where k_1 and k_2 are the rates for acetic acid and propionic acid, respectively, and ΔG_1 and ΔG_2 are the free energy barriers for acetic acid and propionic acid, respectively. The calculated $\Delta G_1 - \Delta G_2$ is −0.02 eV, which results in

$$\frac{k_1}{k_2} = \exp\left(-\frac{-0.02}{k_B T}\right) \approx 2 \quad (11)$$

This is consistent with the experimental data in Figure 2, in which k_1/k_2 = 4.7. It should be noted, though, that the energy differences here are on the order of 0.1 eV, which is less than the accuracy of DFT and within the experimental error limits.

3.6. Density Functional Theory Simulations of DKIE of Unity for Propionate Acid Oxidation. The absence of a DKIE in the experiments carried out herein on propionate and butyrate indicate that the C−H activation steps are not kinetically involved in the overall oxidation process. This is quite different from the results for acetate oxidation which finds a DKIE value of ∼4 which indicates that the C−H bond is kinetically relevant in the oxidation of the acetate. The rate of the oxidation of the larger carboxylate species as presented in Section 3.5 is controlled by the rate of C−O activation, in which the C−H activation steps are either equilibrated or occur after C−O activation. All of the C−H activation steps except for the last one involving $HCCO^{*Au}$ to $Au_2C{=}C{=}O$ occur before C−O bond activation that occurs in the rate-controlling step. The kinetic analyses presented earlier and the microkinetic simulations show that $(OH)OCH{-}CHCOO^{*TiAu}$ intermediate is quasi-equilibrated, and as such, the C−H activation steps involved in its formation do not contribute to the kinetics of ketenylidene formation. As a result, there should be no DKIE for propionic acid or butyric acid oxidation. Microkinetic simulations discussed in Section 3.5 were used to directly simulate the oxidation of H- and D-labeled propionate and reveal that the DKIE of the reaction is equal to 1. The concentrations of CH_3CH_2COO, $CH_2{=}CHCOO$, and C=C=O intermediates plotted vs time (Figure 8) indicate that the ketenylidene formation rates are the same for both the H-labeled propionate and D-labeled propionate, which further confirms the experimental absence of a DKIE for the higher carboxylate species.

Although acetate and propionate oxidative degradation are both controlled by C−O activation steps, they result in rather different DKIE values. The DKIE for acetate is ∼4, which indicates a strong kinetic isotope effect. The DKIE for propionate, on the other-hand, is ∼1, which would indicate the absence of a kinetic isotope effect. The differences are the result of differences in the overall reaction energies for C−H bonds that precede the C−O activation step. Acetate oxidation occurs via the activation of terminal C−H bonds of CH_3COO^{*Ti} to form H_2CCOO^{*TiAu} and $HCCOO^{*TiAu}$ intermediates that are higher in energy and therefore formed by an endothermic process. As such, the reaction is not quasi-equilibrated. As a result, there are differences in the concentration of HCCOO* and DCCOO* intermediates that form on the surface and, thus, differences in the rate of oxidation for the deuterium labeled and unlabeled acetate, even though the reaction is controlled by the rate of C−O activation. The selective oxidation of propionate, on the other hand, rapidly equilibrates to form the stable $(OH)OCH{-}CHCOO^{*TiAu}$ intermediate that subsequently undergoes C−O activation in the rate-limiting step. As such, the C−H bond is not involved in any of the kinetically relevant steps and does not lead to any differences in the concentration of the propionate intermediates in these steps (as shown in Figure 8b,c); therefore, there are no kinetic isotope effects.

3.7. Theoretical Studies of Ketenylidene Hydrogenation. Subsequent DFT calculations were carried out to determine the site for hydrogen addition to the $Au_2C{=}C{=}O$ intermediate for H addition as well as the rates for hydrogenating the ketenylidene, as shown in Figure 9. Hydrogen was found to preferentially attack the terminal C atom of the C=C=O species bonded to the Au over that of the O atom or the central C atom. The second hydrogen also preferentially attacks the terminal C−Au moiety, resulting in the formation of the $H_2C{=}C{=}O$ intermediate that then

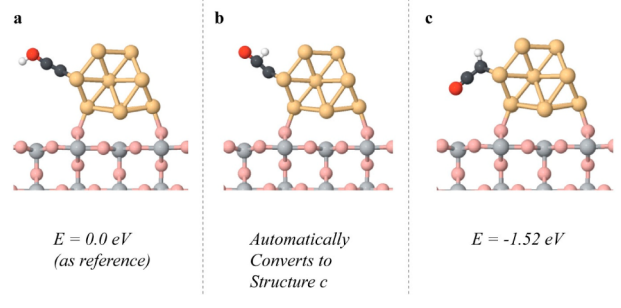

Figure 9. A comparison of the DFT calculated stabilities for the hydrogen addition to (a) the terminal O, (b) the central C, and (c) the end C bound to Au. The Ti atoms, the O in the TiO_2 lattice, adsorbed O, C atoms, and H atoms are shown in gray, pink, red, black, and white, respectively. The energies are reported in electronvolts.

DOI: 10.1021/cs5014255
ACS Catal. 2015, 5, 744−753

desorbs from the surface. The results are consistent with the experimental results, which indicates that the $Au_2C{=}C{=}O$ species can be hydrogenated to form $H_2C{=}C{=}O$, which leaves the surface. However, because the $Au_2C{=}C{=}O$ species remains on the surface during the oxidation reaction and after evacuation, in contrast to ketene, $H_2C{=}C{=}O$, ketene does not appear to be an intermediate in the formation of $Au_2C{=}C{=}O$ because it would readily desorb before undergoing subsequent reaction.

3.8. Pressure and Temperature Dependent Carboxylate Oxidation. The reaction temperatures and pressures for these experiments were chosen to conveniently observe the entire oxidation reaction, including intermediates and the final fully oxidized products. However, repeated experiments at higher O_2 pressures produce the same products but at faster rates, producing higher concentrations of fully oxidized products, such as CO_2 and H_2O. In addition, repeated experiments at higher temperatures also increase the rate of the reaction, with the reactant carboxylates on the surface being consumed until the Au/TiO_2 surface is clean again. The spectra for these experiments are shown in Supporting Information Figure S7.

4. CONCLUSIONS

The reaction paths and the catalytic sites necessary for the oxidative dehydrogenation of propionate and butyrate on the Au/TiO_2 catalyst surface to form $Au_2C{=}C{=}O$ species were examined using in situ IR spectroscopy, kinetic labeling studies, and density functional theoretical calculations. The results were compared with our previous studies on the oxidation of acetic acid over Au/TiO_2 to understand the changes in the reaction mechanism that occur with an increase in the chain length of the acid.

1. The oxidation of propionic and butyric acid proceeds via the dissociative adsorption of the acid on the TiO_2 substrate near the Au/TiO_2 interface to form the carboxylate intermediates (propionate and butyrate) and the activation of the O_2 at the dual Ti^{4+}–Au site (O_2 activation on low coordination Au sites on a Au particle requires a >1 eV barrier). Theoretical calculations suggest that the dehydrogenation of propionate and butyrate intermediates predominantly occurs at the C_α–C_β positions via weakly held basic O adatoms on Au to form acrylate and crotonate species, which is consistent with experimental results that show the formation of these same intermediates.[12]
2. The acrylate and crotonate intermediates can both undergo further oxidation and subsequent C–C and C–O scission to form the ketenylidene product. Theoretical results indicate that this can proceed via (i)nucleophilic addition of basic O or OH intermediates on Au to the unsaturated C=C bonds of acrylate and crotonate; (ii) C–C bond scission at the C_α-C_β position of the partially oxidized acrylate and crotonate intermediates at the dual Au–Ti^{4+}sites; (iii) C–O scission of the $HCCOO^{*TiAu}$ intermediate at the interfacial Au–Ti^{4+} sites; and (iv) O-assisted C–H activation of the $HC{=}C{=}O^{*Au}$ species to form the $Au_2C{=}C{=}O$ species.
2. Kinetic studies of $Au_2C{=}C{=}O$ formation for all three acids at 400 K produced a ~15-fold rate change between acetic and butyric acid. These changes do not appear in the measured activation barriers. Although theoretical simulations suggest that these differences may be due to the changes in entropy and the overall free energies of activation, the calculated energy differences are within the accuracy of density functional theory and its application, thus making it difficult to conclude that the differences are due solely to entropy.
3. Ketenylidene hydrogenation studies to produce $H_2C{=}C{=}O(g)$ rule out the possibility of an adsorbed $H_2C{=}C{=}O$ intermediate species because ketene is only weakly bound on Au/TiO_2 catalysts.
4. A DKIE of unity was determined experimentally and theoretically for propionate and butyrate oxidative dehydrogenation, providing evidence that dehydrogenation steps occur before C–O and C–C bond scission, at the α- and β-carbons of propionate and butyrate. These steps are equilibrated and do not contribute to a DKIE. The rate-limiting step involves C–O bond activation.
5. The oxidation of acetic acid that proceeds via C–H bond activation at its C_α (C2) position is characteristically different from that for the C_3 and higher acids, which proceed via the dehydrogenation at both C_α–C_β (C2–C3) positions to form unsaturated carboxylates. The unsaturated carboxylates can readily undergo further oxidation and subsequent C–C and C–O rupture to form the $HCCOO^{*TiAu}$ intermediate. The acetate intermediate, however, has only C–H bonds at its C_α and therefore cannot form the unsaturated carboxylate or undergo C_α–C_β activation. Instead, for acetic acid, two of the C_α–H bonds are broken in a nonequilibrated process to directly form the same $HCCOO^{*TiAu}$ intermediate that results from the higher acids.
6. The measured activation barriers for the oxidation of acetic, propionic, and butyric acids are all controlled by the activation of the C–O bond and are quite similar. DKIE values, however, are quite different for the oxidation of acetic acid, which involves a strong kinetic isotope effect (DKIE ~ 4) versus propionic and butyric acids, which have negligible effects (DKIE ~ 1). The difference appears to be due to the fact that the $HCCOO^{*TiAu}$ intermediate formed via the oxidation of acetic acid is nonequilibrated but the C_3 and higher acids proceed via the formation of a quasi-equilibrated $HCCOO^{*TiAu}$ intermediate.

■ ASSOCIATED CONTENT

Supporting Information

The following file is available free of charge on the ACS Publications website at DOI: 10.1021/cs5014255

Control experiments on the pure TiO_2 catalyst and further details of the DFT calculations and model (PDF)

■ AUTHOR INFORMATION

Corresponding Author

*E-mail: johnt@virginia.edu.

Notes

The authors declare no competing financial interest.

■ ACKNOWLEDGMENTS

We thank the DOE, Office of Basic Energy Sciences for Grant No. DE-FG02-09ER16080 and support from the FIRST

DOI: 10.1021/cs5014255
ACS Catal. 2015, 5, 744–753

Center, an Energy Frontier Research Center funded by the U.S. Department of Energy, Office of Basic Energy Sciences. We also gratefully acknowledge the XSEDE computing resources from Texas Advanced Computing Center and San Diego Supercomputer Center and the AES Corporation for their support of Monica McEntee via the AES Graduate Fellowships in Energy Research Program at the University of Virginia. We also thank Steve Kalman for his help with the ^{1}H NMR acid purity tests.

REFERENCES

(1) Miranda, M. O.; Pietrangelo, A.; Hillmyer, M. A.; Tolman, W. B. *Green Chem.* **2012**, *14*, 490−494.
(2) Yang, X.; He, Z.; Zhou, X.; Xu, S.; Leung, K. *Appl. Surf. Sci.* **2006**, *252*, 3647−3657.
(3) Schulz, K. H.; Cox, D. F. *J. Phys. Chem.* **1992**, *96*, 7394−7398.
(4) Xu, L.; Xu, Y. *Surf. Sci.* **2010**, *604*, 887−892.
(5) Xu, L.; Xu, Y. *Catal. Today* **2011**, *165*, 96−105.
(6) Davis, J.; Barteau, M. *Langmuir* **1989**, *5*, 1299−1309.
(7) Holz, M. C.; Kähler, K.; Tölle, K.; van Veen, A. C.; Muhler, M. *Phys. Status Solidi B* **2013**, *250*, 1094−1106.
(8) Hansen, E.; Neurock, M. *J. Phys. Chem. B* **2001**, *105*, 9218−9229.
(9) Lu, J.; Behtash, S.; Heyden, A. *J. Phys. Chem. C* **2012**, *116*, 14328−14341.
(10) Green, I. X.; Tang, W.; Neurock, M.; Yates, J. T., Jr. *J. Am. Chem. Soc.* **2012**, *134*, 13569−13572.
(11) Green, I. X.; Tang, W.; Neurock, M.; Yates, J. T., Jr. *Faraday Discuss.* **2013**, *162*, 247−265.
(12) McEntee, M.; Tang, W.; Neurock, M.; Yates, J. T., Jr. *J. Am. Chem. Soc.* **2014**, *136*, 5116−5120.
(13) Rodriguez, J.; Ma, S.; Liu, P.; Hrbek, J.; Evans, J.; Perez, M. *Science* **2007**, *318*, 1757−1760.
(14) Wang, J.; Hammer, B. *Phys. Rev. Lett.* **2006**, *97*, 136107.
(15) Hammer, B.; Norskov, J. *Nature* **1995**, *376*, 238−240.
(16) Kotobuki, M.; Leppelt, R.; Hansgen, D.; Widmann, D.; Behm, R. *J. Catal.* **2009**, *264*, 67−76.
(17) Laursen, S.; Linic, S. *Phys. Chem. Chem. Phys.* **2009**, *11*, 11006−11012.
(18) Rojluechai, S.; Chavadej, S.; Schwank, J. W.; Meeyoo, V. *Catal. Commun.* **2007**, *8*, 57−64.
(19) Green, I. X.; Tang, W.; Neurock, M.; Yates, J. T., Jr. *Angew. Chem., Int. Ed.* **2011**, *50*, 10186−10189.
(20) Green, I. X.; Tang, W.; Neurock, M.; Yates, J. T., Jr. *Science* **2011**, *333*, 736−739.
(21) Green, I. X.; Tang, W.; McEntee, M.; Neurock, M.; Yates, J. T., Jr. *J. Am. Chem. Soc.* **2012**, *134*, 12717−12723.
(22) Boccuzzi, F.; Chiorino, A.; Manzoli, M.; Lu, P.; Akita, T.; Ichikawa, S.; Haruta, M. *J. Catal.* **2001**, *202*, 256−267.
(23) Haruta, M.; Tsubota, S.; Kobayashi, T.; Kageyama, H.; Genet, M. J.; Delmon, B. *J. Catal.* **1993**, *144*, 175−192.
(24) Date, M.; Haruta, M. *J. Catal.* **2001**, *201*, 221−224.
(25) Kung, H.; Kung, M.; Costello, C. *J. Catal.* **2003**, *216*, 425−432.
(26) Kung, M. C.; Davis, R. J.; Kung, H. H. *J. Phys. Chem. C* **2007**, *111*, 11767−11775.
(27) Molina, L.; Rasmussen, M.; Hammer, B. *J. Chem. Phys.* **2004**, *120*, 7673.
(28) Green, I. X.; McEntee, M.; Tang, W.; Neurock, M.; Yates, J. T., Jr. *Top. Catal.* **2013**, *56*, 1512−1524.
(29) Basu, P.; Ballinger, T.; Yates, J. T., Jr. *Rev. Sci. Instrum.* **1988**, *59*, 1321−1327.
(30) Zanella, R.; Giorgio, S.; Henry, C. R.; Louis, C. *J. Phys. Chem. B* **2002**, *106*, 7634−7642.
(31) Kresse, G. *Phys. Rev. B* **2000**, *62*, 8295.
(32) Perdew, J. P.; Wang, Y. *Phys. Rev. B* **1992**, *45*, 13244.
(33) Blöchl, P. E. *Phys. Rev. B* **1994**, *50*, 17953.
(34) Kresse, G.; Joubert, D. *Phys. Rev. B* **1999**, *59*, 1758.
(35) Dudarev, S.; Botton, G.; Savrasov, S.; Humphreys, C.; Sutton, A. *Phys. Rev. B* **1998**, *57*, 1505.
(36) Morgan, B. J.; Watson, G. W. *Surf. Sci.* **2007**, *601*, 5034−5041.
(37) Liao, L. F.; Lien, C. F.; Lin, J. L. *Phys. Chem. Chem. Phys.* **2001**, *3*, 3831−3837.
(38) Hasan, M.; Zaki, M.; Pasupulety, L. *Appl. Catal., A* **2003**, *243*, 81−92.
(39) Mattsson, A.; Osterlund, L. *J. Phys. Chem. C* **2010**, *114*, 14121−14132.
(40) Chen, Y. K.; Lin, Y. F.; Peng, Z. W.; Lin, J. L. *J. Phys. Chem. C* **2010**, *114*, 17720−17727.
(41) Li, N.; Sun, S. *J. Electroanal. Chem.* **1997**, *436*, 65−72.
(42) Weng, Z.; Ni, X.; Yang, D.; Wang, J.; Chen, W. *J. Photochem. Photobiol., A* **2009**, *201*, 151−156.
(43) Sondag, A. H. M.; Raas, M. C.; Van Velzen, P. N. T. *Chem. Phys. Lett.* **1989**, *155*, 503−510.
(44) Thomas, A. G.; Syres, K. L. *Chem. Soc. Rev.* **2012**, *41*, 4207−4217.
(45) Gutiérrez-Sosa, A.; Martínez-Escolano, P.; Raza, H.; Lindsay, R.; Wincott, P. L.; Thornton, G. *Surf. Sci.* **2001**, *471*, 163−169.
(46) Wendt, S.; Sprunger, P. T.; Lira, E.; Madsen, G. K.; Li, Z.; Hansen, J. Ø; Matthiesen, J.; Blekinge-Rasmussen, A.; Lægsgaard, E.; Hammer, B. *Science* **2008**, *320*, 1755−1759.
(47) Zhang, Z.; Lee, J.; Yates, J. T., Jr; Bechstein, R.; Lira, E.; Hansen, J. Ø; Wendt, S.; Besenbacher, F. *J. Phys. Chem. C* **2010**, *114*, 3059−3062.
(48) Liu, X.; Madix, R. J.; Friend, C. M. *Chem. Soc. Rev.* **2008**, *37*, 2243−2261.
(49) Roldan, A.; Torres, D.; Ricart, J. M.; Illas, F. *J. Mol. Catal. A: Chem.* **2009**, *306*, 6−10.
(50) Xu, B.; Liu, X.; Haubrich, J.; Madix, R. J.; Friend, C. M. *Angew. Chem., Int. Ed.* **2009**, *48*, 4206−4209.
(51) Madix, R. J.; Auerbach, D. *Surface reactions*; Springer-Verlag: New York, 1994; Vol. *34*, p 5−53.
(52) Zope, B. N.; Hibbitts, D. D.; Neurock, M.; Davis, R. J. *Science* **2010**, *330*, 74−78.
(53) Camellone, M. F.; Zhao, J.; Jin, L.; Wang, Y.; Muhler, M.; Marx, D. *Angew. Chem., Int. Ed.* **2013**, *52*, 5780−5784.
(54) Sim, W.; King, D. *J. Phys. Chem.* **1996**, *100*, 14794−14802.
(55) Mul, G.; Zwijnenburg, A.; van der Linden, B.; Makkee, M.; Moulijn, J. A. *J. Catal.* **2001**, *201*, 128−137.

DOI: 10.1021/cs5014255
ACS Catal. 2015, 5, 744−753